Mineralogical Magazine (2023), **87**, 896–907
doi:10.1180/mgm.2023.70

CAMBRIDGE UNIVERSITY PRESS

Article

Narsarsukite in peralkaline granites from the Papanduva Pluton, Graciosa Province, south Brazil: Insights from textural and compositional features

Silvio R.F. Vlach[1] and Frederico C.J. Vilalva[2]

[1]Department of Mineralogy and Geotectonics, University of São Paulo, São Paulo, SP, 05508-080, Brazil and [2]Department of Geology, Federal University of Rio Grande do Norte, Natal, RN, 59078-970, Brazil

Abstract

We report textural and compositional data for the titanosilicate narsarsukite [$Na_2(Ti,Fe^{3+})Si_4(O,F)_{11}$] in peralkaline granites from the Papanduva Pluton in Graciosa Province, south-southeastern Brazil. Two distinct narsarsukite generations, one late magmatic and the other post-magmatic, were identified on the basis of textural and compositional features. The magmatic generation consists of larger, euhedral to subhedral variably zoned crystals and late poikilitic intergrowths between narsarsukite and albite laths, representing the crystallisation of the latest melt pockets. The post-magmatic generation forms smaller, typically fibrous crystals and irregular aggregates that occur interstitially or replace the primary mafic minerals, particularly arfvedsonite. Compositions of narsarsukite from the Papanduva Pluton cover most of the compositional range described in known occurrences. The magmatic generation is enriched in Zr and depleted in Al. The Fe^{3+} and Al contents show a positive correlation for the magmatic crystals, but a negative correlation for the post-magmatic narsarsukite. The Al/Fe^{3+} ratios are higher in the post-magmatic crystals and can be used to discriminate between the two generations. The compositional variations are controlled mainly by the heterovalent substitution $(Ti, Zr)^{4+} + O^{2-} = (Al, Fe)^{3+} + F^{1-}$, and are compatible with $(OH)^{1-}$ ions in the O site. Narsarsukite has significantly higher concentrations of mid REE+Y and HFSE and very low to absent contents of LREE and LILE relative to the host-rocks. The average REE pattern of the magmatic crystals is highly fractionated, consistent with the expected strong preference for the smaller HREE. The post-magmatic crystals that replace arfvedsonite have flatter patterns, with higher concentrations of LREE and MREE. Their compositions suggest a fluid phase relatively rich in HFSE, REE, Y, Pb, Th and U. Narsarsukite is a common phase in strongly peralkaline granites such as the Papanduva Pluton and the well-known Strange Lake Complex, and should be considered a diagnostic mineral of highly peralkaline SiO_2-oversaturated rocks containing rare Ti and Zr mineral assemblages.

Keywords: narsarsukite; compositions; REE patterns; peralkaline granites; Papanduva Pluton; Graciosa Province; Brazil

(Received 4 April 2023; accepted 24 August 2023; Accepted Manuscript published online: 12 September 2023; Associate Editor: Edward Sturgis Grew)

Introduction

Titano- and zirconosilicates are typical phases constituting the mafic mineral assemblages of highly peralkaline SiO_2-undersaturated and -oversaturated rocks and contribute to the chemical budget of the high-field-strength elements (HFSE), the rare earth elements (REE) and Y during the evolution of these systems in both the magmatic and post-magmatic crystallisation stages. Furthermore, mineral assemblages and compositions may give relevant clues to access the main intensive parameters of these crystallisation environments, as well as the alkalinity and volatile fugacities in the magma (e.g. Nichols and Carmichael, 1969; Marks *et al.*, 2011; Andersen *et al.*, 2010; Siachoque *et al.*, 2022).

Corresponding author: Silvio R.F. Vlach; Email: srfvlach@usp.br
Cite this article: Vlach S.R.F. and Vilalva F.C.J. (2023) Narsarsukite in peralkaline granites from the Papanduva Pluton, Graciosa Province, south Brazil: Insights from textural and compositional features. *Mineralogical Magazine* **87**, 896–907. https://doi.org/10.1180/mgm.2023.70

Among the known titanosilicates, narsarsukite is a relatively rare inosilicate with the IMA accepted formula $Na_2(Ti,Fe^{3+})Si_4(O,F)_{11}$, crystallising in the *I*4/*m* space group (e.g. Anthony *et al.*, 2003). It was first described in a pegmatite from Narsarsuk, Greenland, by Flink (1901) and its crystal structure was determined by Pyatenko and Pudovkina (1960) and Peacor and Buerger (1962). Recently, Schingaro *et al.* (2017) revisited the narsarsukite structure and suggested the extended formula $Na_4\{Ti^{4+}_{1-x},M_x^{3+})[O_{1-x}(OH,F)_x]\}_2(Si_8O_{20})$ with $0 < x \leq 1$. The structure is composed of 4-periodic double chains of $[Si_4O_{10}]_2$ tetrahedra connected into tubes and to chains of corner-sharing $Ti(O_5,OH,F)$-octahedra. The tubes are parallel to the c-axis, and the 7-coordinated Na^+ cations are located in the cavities between the tubes and the octahedral chains. According to the structure hierarchy of the chain-, ribbon- and tube-silicates developed by Day and Hawthorne (2020), based on the connectedness of one-dimensional polymerisation of the $(TO_4)^{n-}$ tetrahedra, the narsarsukite structure belongs to the $^3T_8$ group. This means that the connectivity of the $[SiO_4]^{4-}$ tetrahedron has a value of 3 and the number of these tetrahedra is 8 in the repeat structural unit.

© The Author(s), 2023. Published by Cambridge University Press on behalf of The Mineralogical Society of the United Kingdom and Ireland

https://doi.org/10.1180/mgm.2023.70 Published online by Cambridge University Press

Narsarsukite occurs in several volcanic and plutonic, mainly SiO_2-oversaturated, peralkaline rocks, pegmatites and hornfels. It is associated commonly, in addition to quartz and alkali-feldspars, with aegirine, arfvedsonite, pectolite, various titanosilicates, such as aenigmatite, astrophyllite, neptunite and bafertisite, and zirconosilicates, such as elpidite (e.g. Birkett *et al.*, 1996; Siachoque *et al.*, 2022).

The main crystallochemical features of narsarsukite are well-established in the mineralogical literature (e.g. Wagner *et al.*, 1991; Read, 1991; Birkett *et al.*, 1996; Schingaro *et al.*, 2017). Wagner *et al.* (1991) discussed infrared and Mössbauer spectroscopic results, whereas Schingaro *et al.* (2017) provided micro-Fourier transform infrared and X-ray photoelectron spectroscopy data. Eu^{3+}-doped narsarsukite was synthesised by the sol-gel method (e.g. Balmer *et al.*, 1997) and was shown to have luminescence properties (Rainho *et al.*, 2003).

Notwithstanding the wealth of data available on narsarsukite, there is a paucity of systematic studies that combine textural and compositional features, particularly those comparing the characteristics of magmatic and post-magmatic crystallisation generations. These are relevant aspects to consider, as more than one textural generation of the mafic minerals (e.g. magmatic vs. hydrothermal) is common in peralkaline rocks (e.g. Siachoque *et al.*, 2022). Additionally, although some electron microprobe data for Y and Ce have been made by Read (1991) and Birkett *et al.* (1996), REE data are still scarce and complete analyses exist only for peralkaline granites from the Strange Lake Complex (Vasyukova and Williams-Jones, 2019).

Narsarsukite is a common and widespread accessory mineral in the strongly peralkaline alkali-feldspar granites of the Papanduva Pluton, Morro Redondo Complex, in the Neoproterozoic A-type Graciosa Province, south-southeastern Brazil (Gualda and Vlach, 2007). This work presents and discusses textural and compositional data (major, minor and trace elements) for magmatic and post-magmatic narsarsukite generations. We also examine the behaviour of REE in this mineral and contribute to the mineralogical knowledge of the province and similar occurrences worldwide.

The Papanduva Pluton

The Papanduva Pluton, with ~60 km^2 and irregular surface contours (Fig. 1), is a peralkaline intrusion of the Morro Redondo Complex in the Neoproterozoic (*ca.* 580 Ma) Graciosa Province, south-southeastern Brazil (Gualda and Vlach, 2007; Vlach *et al.*, 2011; Vilalva and Vlach, 2014; Vilalva *et al.*, 2019). The pluton is composed of slightly greyish hypersolvus holo- to leucocratic alkali-feldspar granites showing significant variations in structure, texture and mineralogy. These variations have been grouped and mapped as massive, cataclastic, and foliated fine-, medium- and coarse-grained petrographic facies, accompanied by some microgranites. See Vilalva (2007), Vilalva and Vlach

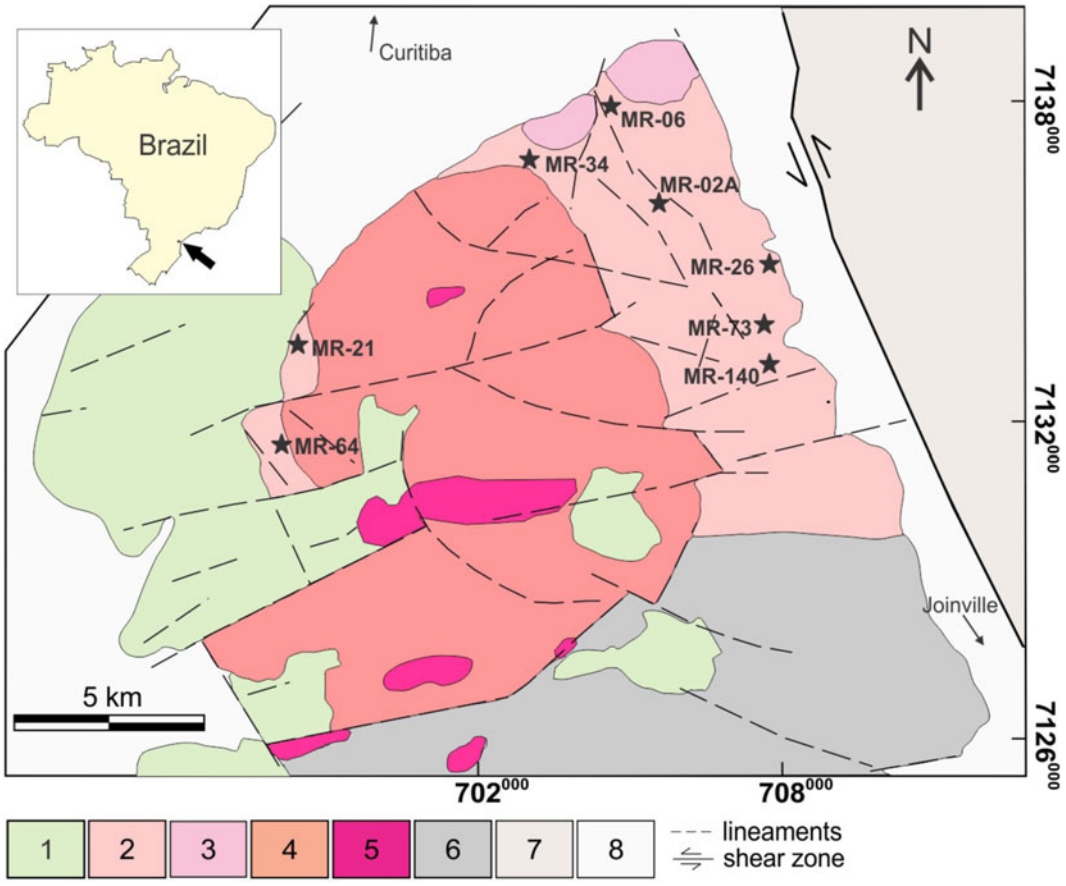

Figure 1. Simplified geological map of the Papanduva Pluton, Morro Redondo Complex, South Brazil. (1) Silicic and basic-intermediate volcanics associated with the intrusive rocks; granitic petrographic facies: (2) foliated; (3) cataclastic; (4) massive and (5) microgranites. (6) Metaluminous to slightly peraluminous syeno- and monzogranites from the Quiriri Pluton. (7) Metasediments from the Paranaguá Terrain; (8) gneisses and granulites from the Luis Alves microplate. Asterisks indicate locations of the samples analysed. Modified from Vilalva and Vlach (2014).

https://doi.org/10.1180/mgm.2023.70 Published online by Cambridge University Press

(2014) and Vilalva *et al.* (2016) for detailed petrographic descriptions and textural and compositional characterisation of the rock-forming felsic and mafic minerals. The granites are highly ferroan [$FeO^T/(FeO^T+MgO) \geq 0.96$], and have SiO_2 contents of 74–78 wt.% and Na_2O+K_2O contents of 8.9–9.3 wt.%. The peralkaline index [$(Na_2O+K_2O)/Al_2O_3$ molar] is between 1.04 and 1.28, and the HFSE contents are relatively high, up to 2430 ppm (Vilalva and Vlach, 2014).

The most evolved and highly peralkaline foliated facies (Fig. 2) have sub-magmatic, close-to-solidus, deformational structures with variable intensity. They have a fine- to medium-grained porphyroclastic to protomylonitic textures, with orientated and deformed megacrysts of mesoperthite, arfvedsonite and quartz in a fine-grained, sometimes saccharoidal, matrix with alkali-feldspars (microcline and albite), quartz and mafic minerals. Millimetric miarolitic cavities or vugs (partially filled with accessory phases) occur in some samples. In most hand samples, yellowish minerals (mainly narsarsukite and zirconosilicates) can be seen. The accessory and rare phases include earlier-, late- and/or post-magmatic generations of aenigmatite, astrophyllite, narsarsukite, elpidite and other unidentified zirconosilicates of Na and K, neptunite, britholite-(Ce), nacareniobsite-(Ce), turkestanite, bastnäsite-(Ce), allanite-(Ce), titanite, anatase, together with fluorite and several unidentified phases (see Vilalva and Vlach, 2010, Vilalva *et al.*, 2013; Siachoque *et al.*, 2022). Siachoque *et al.* (2022) present an interpretation for the relative sequence of crystallisation of these minerals based on textural evidence. Narsarsukite is the most abundant rare accessory mineral in these rocks, reaching up to 3.2 vol.%.

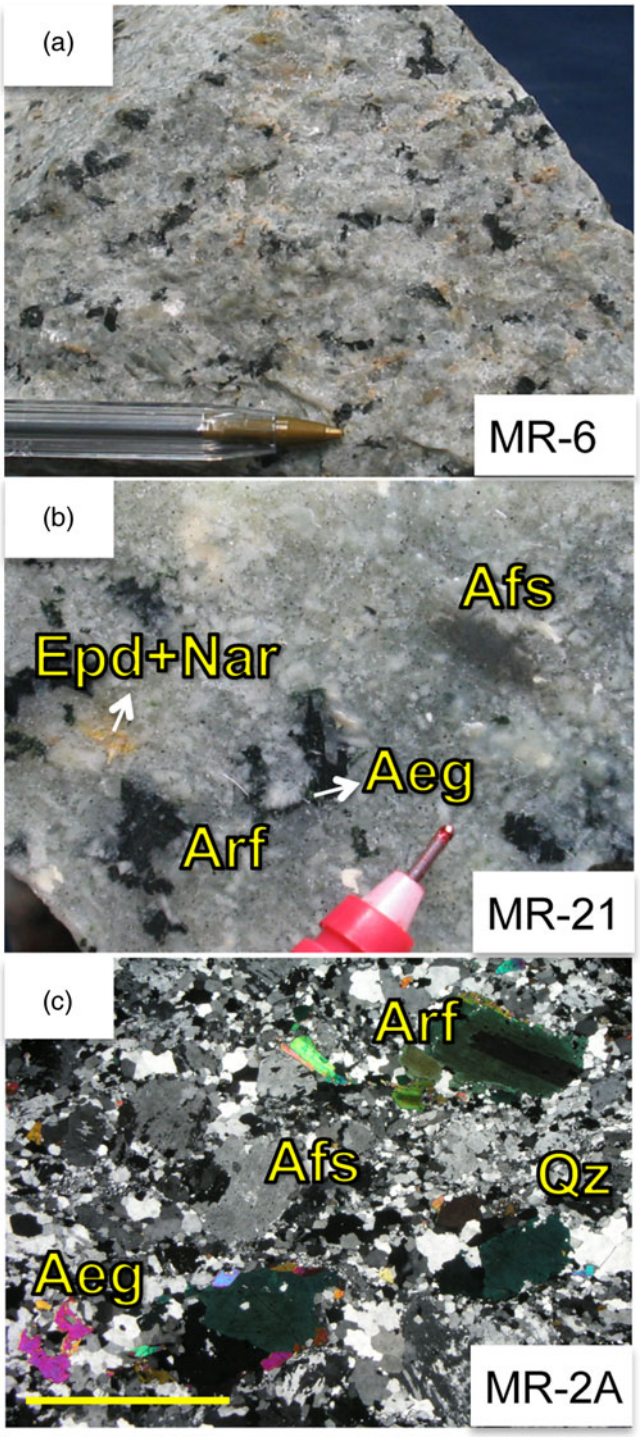

Figure 2. (a) and (b) General structural and textural aspects of the peralkaline alkali-feldspar granites from the foliated facies of the Papanduva Pluton; (c) texture of the most deformed rock type under the microscope with crossed polarisers, showing mesoperthitic alkali-feldspar, quartz and arfvedsonite (commonly zoned) porphyroclasts in a recrystallised matrix with quartz, alkali-feldspars (microcline and albite) and mafic minerals. Yellow bar in (c) measures 1 mm. Mineral abbreviations as recommended by the IMA (Warr, 2021).

Samples and analytical procedures

The analytical work was carried out at the GeoAnalitica facility, Institute of Geosciences, University of São Paulo. After conventional petrographic analysis, seven samples from the foliated facies were chosen for major, minor and some trace-element analysis with the electron microprobe analyser (EMPA). Three of these samples were further analysed for trace elements using laser ablation inductively coupled plasma mass spectrometry (LA-ICP-MS). The locations of the samples are shown in Fig. 1.

Electron microprobe analyses

Electron microprobe analyses were performed using the JEOL-JXA8600S and JEOL JXA-FE8530 electron microprobes. The latter instrument is equipped with a field emission electron gun. Both these instruments have five wavelength dispersive (WD) and one energy dispersive (ED) spectrometers. Quantitative WDS spot analysis was performed with the JEOL-JXA8600S equipment, and compositional mapping was obtained using a combination of WDS and EDS signals with the JEOL JXA-FE8530 equipment. The WDS analytical conditions were 15 kV, 20 nA and 5–10 μm for the column accelerating voltage, beam current and diameter, respectively. The analytical routine is summarised in Supplementary Table S1. Fluorine and Na were measured simultaneously in the first spectrometric round to minimise their loss. The matrix effect correction and conversion of the raw data to mass oxides were performed using *PROZA* software (Bastin and Heijligers, 1990). The analytical errors, checked against standards readings, are lower than 2% relative for the major, between 5 and 10% relative for the minor, and higher for trace elements. Back-scattered electron (BSE) images and compositional maps were obtained with a focused beam and the same analytical conditions. The dwell time for maps was set to 50 ms.

https://doi.org/10.1180/mgm.2023.70 Published online by Cambridge University Press

Literature data suggest that Fe in narsarsukite occurs mainly as Fe^{3+} (Wagner *et al.*, 1991; Birkett *et al.*, 1996; Schingaro *et al.*, 2017). Its structural formula has been alternatively computed considering seven total cations or 11 (O+F). The first scheme does not account for potential vacancies in the Na site (Wagner *et al.*, 1991) and might result in some excess in the Si and Ti sites in addition to in the O site, and the second scheme does not allow for the possible entry of $(OH)^{1-}$ anions in the structure. Considering these drawbacks, we computed the structural formulae according to both approaches. We used the first scheme for the analytical data to better examine the substitution of O^{2-} by F^{-1} in the O sites.

Laser ablation inductively coupled plasma mass spectrometry analysis

Laser ablation inductively coupled plasma mass spectrometry analysis was performed using Quadrupole Elan 6100DRC equipment from Perkin Elmer coupled with a UP-213 laser ablation system from NewWave Research, provided with a 213 nm Nd-doped YAG laser, following the procedures described in Andrade (2016). The analyses were carried out in raster mode with spot sizes varying from 30 to 50 μm. Back-scattered electron images were used to guide the selection of areas to be analysed.

The laser beam fluence and repetition rate were set at 8.5 J/cm^2 and 4 Hz, respectively. The following isotopes were measured: ^{7}Li, ^{9}Be, ^{25}Mg, ^{31}P, ^{42}Ca, ^{45}Sc, ^{49}Ti, ^{51}V, ^{52}Cr, ^{55}Mn, ^{59}Co, ^{65}Cu, ^{66}Zn, ^{69}Ga, ^{85}Rb, ^{88}Sr, ^{89}Y, ^{90}Zr, ^{93}Nb, ^{95}Mo, ^{118}Sn, ^{133}Cs, ^{137}Ba, ^{139}La, ^{140}Ce, ^{141}Pr, ^{143}Nd, ^{147}Sm, ^{151}Eu, ^{155}Gd, ^{159}Tb, ^{163}Dy, ^{165}Ho, ^{166}Er, ^{169}Tm, ^{173}Yb, ^{175}Lu, ^{179}Hf, ^{181}Ta, ^{208}Pb, ^{232}Th and ^{238}U. The total acquisition time was set to 120 s, distributed equally between blank and ion signal measures. The signal integration and dwell times were 8.33 and 1.66 ms, respectively. The daily rate of oxide generation was controlled holding ThO^{+} formation below 1%. *Glitter* software (Griffin *et al.*, 2008) was used for data acquisition, treatment, and conversions to concentrations. The synthetic NIST glass SRM-610 and the average TiO_2 content previously measured by WDS were used as external and internal standards, respectively.

Regardless of our efforts, reliable quantitative trace-element data for the post-magmatic narsarsukite generation was

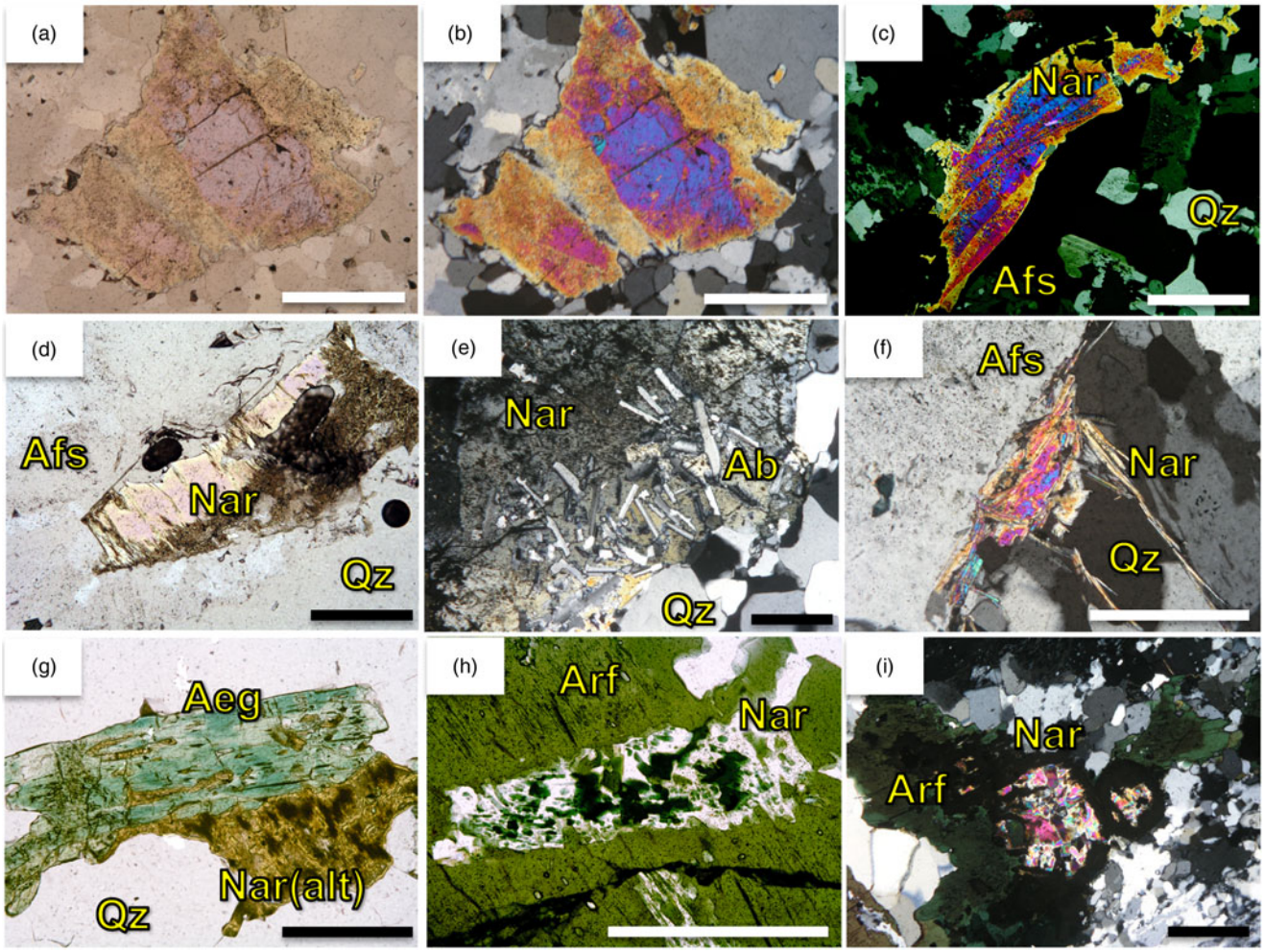

Figure 3. Main textural features of magmatic and post-magmatic narsarsukite generations from the Papanduva Pluton, Graciosa Province. (a) Larger magmatic crystals showing colour zoning and abundant minute inclusions in the yellow–orange intermediate zone, in plane-polarised light; (b) same crystal with cross polarisers, depicting the high birefringence mainly in crystal cores; (c) deformed crystal, bent around a quartz porphyroclast and with some translational slip; (d) zoned crystal partially altered by secondary mineral aggregates; (e) partially altered narsarsukite intergrown with albite laths; (f) post-magmatic lamellar and fibrous crystals associated with a somewhat sizeable magmatic crystal; (g) completely altered crystal associated with aegirine, note narsarsukite (probably post-magmatic) development along aegirine fractures and cleavage; (h) irregular post-magmatic narsarsukite replacing arfvedsonite; (i) crystal aggregate of narsarsukite replacing arfvedsonite. Images (d) (g) and (h) are plane-polarised light, images (c), (e), (f) and (i) are under crossed polarisers. White and black scale bars measure 0.5 mm.

https://doi.org/10.1180/mgm.2023.70 Published online by Cambridge University Press

considerably more difficult to acquire. This is because of the small dimensions of the crystals, their common lamellar or fibrous habit, and their close association with arfvedsonite and aegirine. We were only able to obtain two reliable analyses, which were for crystals replacing arfvedsonite. Most of the other analyses were discarded as the measured Ca and Mg contents were relatively high, well above 400 and 300 ppm, respectively, and thus were considered to be mixed, non-representative values.

Results

Textural features

Two generations of narsarsukite were identified on the basis of their textural and compositional features. The most typical characteristics of each generation, as observed under the petrographic microscope, are shown in Fig. 3.

The first generation occurs as interstitial euhedral to subhedral (1–2 mm long) crystals formed during the late-magmatic crystallisation stage and show some textural features similar to those described for narsarsukite in the Strange Lake granites (Birkett *et al.*, 1996). These crystals have platy to tabular habits ($a >> c$) with high relief and second-order birefringence colours, with a weak colourless to pinkish pleochroism. Most larger crystals are zoned, with pinkish colours, high birefringence in their cores, and almost colourless and lower birefringence rims (Fig. 3a–d). Some crystals have a relatively homogenous and clean core surrounded by an intermediate poikilitic zone populated with a significant number of minute inclusions and a thin clean rim (Fig. 3a,b; cf. also Fig. 4). Deformed (bent and with some translational slip features) crystals are common (Fig. 3c). These crystals are very susceptible to alteration and several samples have been replaced by tiny brownish aggregates composed of late alteration minerals, including titanite, bastnäsite, phyllosilicate minerals and other unidentified phases. A remarkable texture observed in interstitial and relatively smaller crystals and in the intermediate and sometimes the rim zones of larger crystals, is a poikilitic intergrowth between narsarsukite and euhedral to subhedral albite laths (Fig. 3e).

The second generation consists of tiny crystals (≤ 1 mm long) with subhedral, lamellar and fibrous habits and seems to be less susceptible to late alteration. They occur mainly as minute inclusions in recrystallised quartz rims, as isolated crystals or crystal aggregates developed along the contacts between the other minerals (Fig. 3f), along fractures and cleavage planes of arfvedsonite and aegirine (Fig. 3g,h) or as irregular aggregates within arfvedsonite (Fig. 3i). The observed textural relationships, particularly those shown in Fig. 3h,i indicate that this generation replaces previous arfvedsonite and possibly aegirine.

A back-scattered electron image and qualitative compositional maps for Ti, Zr, Al, Fe and Nb for the magmatic crystals depicted in Fig. 3a,b are presented in Fig. 4. The images show the main

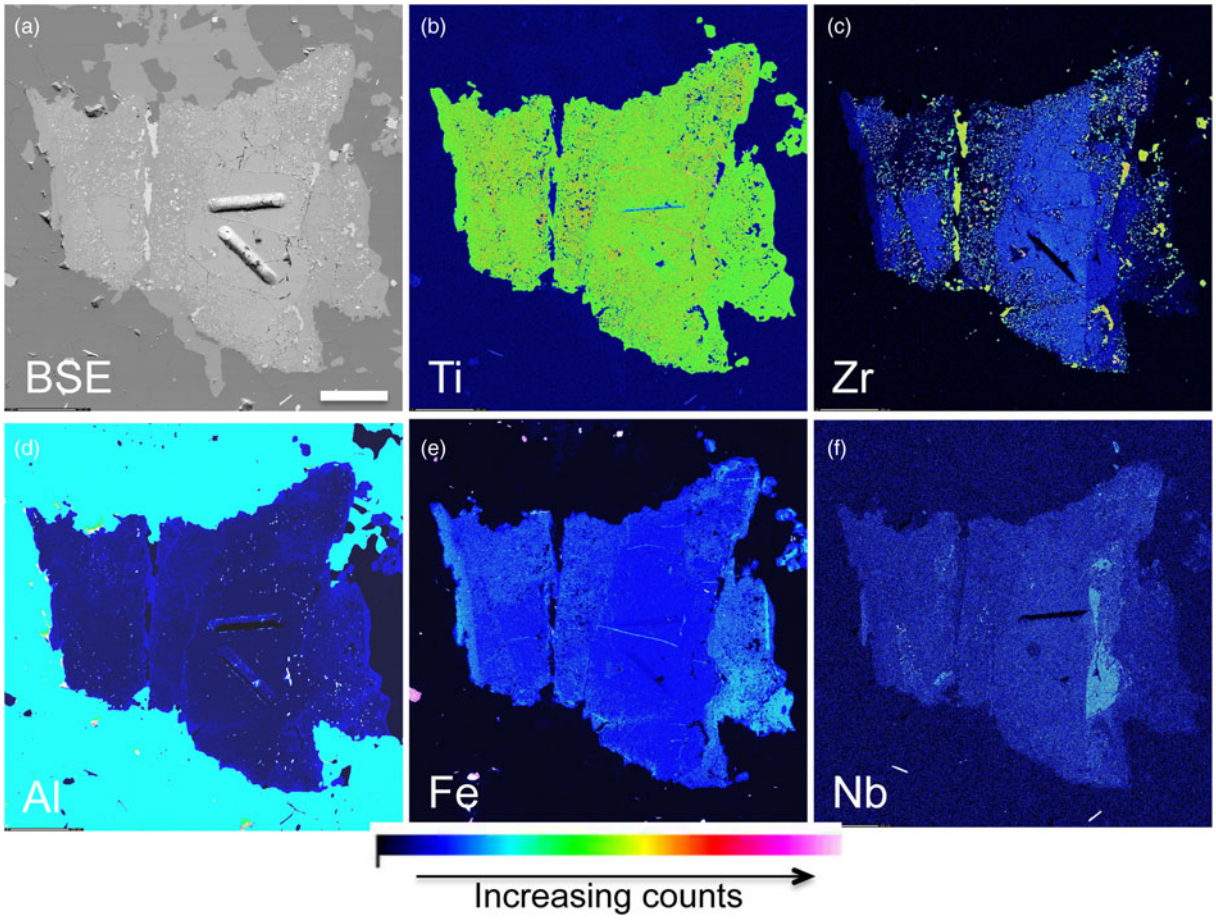

Figure 4. BSE and compositional maps for the narsarsukite crystal shown in Fig. 3a,b. (a) BSE image (compositional mode); (b), (c), (d), (e) and (f) compositional maps for the indicated elements. EDS signals for Ti and WDS signals for the other elements are represented. The two elongated pits, which are most evident in the BSE images, are laser ablation raster lines. The white bar in the BSE image measures 250 μm; the colour bar represents signal intensities. See text.

https://doi.org/10.1180/mgm.2023.70 Published online by Cambridge University Press

zoning pattern observed in most large narsarsukite crystals, with relatively Zr- and Nb-rich and Fe- and Al-poor crystal cores. The poikilitic intermediate and the external rim crystalline zones are almost Zr-free. Furthermore, some areas have irregular Fe and Nb (sectorial?) zoning. The high-Zr and low-Ti phase intergrowth with narsarsukite in the intermediate poikilitic zone is an unidentified zirconosilicate with some Na and K, as determined from EDS qualitative analysis. This intergrowth might alternatively represent the co-precipitation of narsarsukite and a zirconosilicate still in the magmatic stage, indicating the saturation of alkali-bearing zirconosilicates in the melt or fluid-induced post-magmatic exsolution of the Zr-rich phase leaving a Zr-poor narsarsukite host. The most external and Ti-, Al-rich zones might represent late- to post-magmatic overgrowths.

Compositions and variability

Representative compositions for magmatic and post-magmatic narsarsukite are given in Tables 1 (WDS) and 2 (LA-ICP-MS). The complete dataset is given in Supplementary Tables S2 and S3, including structural formulae computed on the basis of seven cations and 11 (O+F) for the WDS data, and analytical errors and average standard readings (SRM-610 and SRM-612, from NIST, and BCR-2G, from USGS) used for analytical control for the LA-ICP-MS data.

The most significant compositional variations are observed for Zr, Al, Fe^{3+} and Nb, all of which occupy the octahedral [Ti]-site. The contents (wt.%) of ZrO_2, Al_2O_3, Fe_2O_3 and Nb_2O_5 vary in the ranges 5.95–0.28, 0.96–0.39, 7.24–3.75, 1.21–0.08, respectively, in the magmatic narsarsukite, and in the ranges 0.27–0.00, 3.10–0.50, 7.42–4.17, 0.76–0.00, respectively, in the post-magmatic narsarsukite. The magmatic generation is richer in Zr and, on average, poorer in Al compared to the post-magmatic generation. Among the divalent cations, MnO has concentrations lower than 0.12 and is higher in magmatic crystals. BaO and CaO are lower than 0.16, and their contents lie in similar ranges in both generations, whereas K_2O is ≤ 0.15 (all quantities in wt.%).

The variations of Al and Fe^{3+} with Zr are shown in Fig. 5a. A slight decrease of both Al and Fe^{3+} with increasing Zr is observed in the compositional zoning of the larger crystals of the magmatic generation. These compositional relationships strongly support the textural interpretations that indicate two contrasted crystallisation generations. In addition to its higher contents, Al also has a significantly wider variation range in the post-magmatic crystals. The Al/Fe^{3+} ratio is a suitable variable to discriminate between narsarsukite generations in the Papanduva Pluton, being almost constant around 0.2 in the magmatic generation and between 0.2 and 1.2 in the post-magmatic generation. Notably, Al and Fe^{3+} contents show a positive correlation in the magmatic crystals, but a negative correlation in the post-magmatic crystals (Fig. 5b). The Fe^{3+} contents in narsarsukite reached maximum values at the transition between the magmatic and post-magmatic crystallisation stages. In the first case, Al and Fe^{3+} increase at an almost constant ratio of 1:4, a feature observed

Table 1. Representative compositions (WDS, wt.%) and atomic proportions for narsarsukite from the Papanduva Pluton, Graciosa Province, south-southeastern Brazil.*

Sample	MR-02A	MR-02A	MR-06	MR-21	MR-34	MR-02A	MR-02A	MR-06	MR-26	MR-02A	MR-140
ID	1,c	1,i	1,r	1,i	1,pk	2,r	2,c	2,r	2,r	2,ra	2,ra
SiO_2	61.28	61.45	62.31	62.01	61.54	62.45	60.73	62.22	62.21	62.63	62.58
ZrO_2	4.40	2.51	0.75	1.52	1.84	0.00	0.17	0.15	0.12	0.22	0.21
TiO_2	13.11	12.40	12.06	13.55	13.24	12.16	11.61	11.54	12.12	12.97	12.68
Al_2O_3	0.39	0.71	0.77	0.62	0.69	2.11	1.04	1.31	2.06	1.88	2.79
Fe_2O_3	3.99	6.01	6.98	5.03	5.30	5.19	6.83	6.71	5.52	5.24	4.41
MnO	0.09	0.06	0.06	0.04	0.08	n.d.	0.06	n.d.	0.02	n.d.	n.d.
MgO	0.01	n.d.	n.d.	n.d.	n.d.	n.d.	n.d.	n.d.	n.d.	n.d.	n.d.
CaO	n.d.	n.d.	n.d.	n.d.	0.02	n.d.	0.02	n.d.	n.d.	n.d.	0.02
BaO	0.10	n.d.	n.d.	n.d.	0.04	n.d.	n.d.	n.d.	0.02	0.05	n.d.
Na_2O	15.08	15.65	16.09	16.00	15.72	16.08	15.57	15.86	15.85	15.95	16.04
K_2O	0.10	0.10	0.02	0.07	0.07	0.03	0.04	0.07	0.04	0.03	0.07
Nb_2O_5	0.38	0.22	0.21	0.43	0.14	n.d.	0.44	0.07	0.16	0.49	0.07
F	0.79	0.91	1.16	1.20	1.53	1.46	0.98	1.33	1.85	1.39	0.94
Sum	99.72	100.02	100.41	100.47	100.21	99.48	97.47	99.25	99.97	100.84	99.80
O=F	0.33	0.38	0.49	0.50	0.64	0.62	0.41	0.56	0.78	0.58	0.40
Total	99.39	99.64	99.92	99.96	99.57	98.86	97.06	98.69	99.19	100.25	99.40
Atomic proportions on the basis of 7 cations											
Si	4.031	3.984	3.992	3.989	3.992	4.003	3.995	4.017	4.001	3.991	3.980
Zr	0.141	0.079	0.023	0.048	0.058	0.000	0.006	0.005	0.004	0.007	0.006
Ti	0.648	0.605	0.581	0.656	0.646	0.586	0.574	0.560	0.586	0.622	0.606
Al	0.030	0.055	0.058	0.047	0.052	0.159	0.080	0.099	0.156	0.141	0.209
FeIII	0.197	0.293	0.336	0.244	0.259	0.250	0.338	0.326	0.267	0.251	0.211
Mn	0.005	0.003	0.003	0.002	0.005		0.003		0.001		
Mg	0.001										
Ca					0.001		0.001				0.002
Ba	0.002				0.001				0.001	0.001	
Na	1.923	1.967	1.998	1.996	1.976	1.998	1.986	1.986	1.976	1.971	1.978
K	0.009	0.008	0.002	0.006	0.006	0.002	0.003	0.006	0.003	0.002	0.005
Nb	0.011	0.006	0.006	0.012	0.004	0.000	0.013	0.002	0.005	0.014	0.002
F	0.164	0.187	0.235	0.244	0.313	0.296	0.203	0.272	0.377	0.279	0.190
O	10.895	10.864	10.802	10.855	10.866	10.794	10.810	10.801	10.820	10.850	10.815

*All Fe as Fe_2O_3; n.d. = not detected; 1= magmatic, 2 = post-magmatic; c = core, i = intermediate and r = crystalline rim zones; pk = poikilitic, ra = replacing arfvedsonite. See also Supplementary Table S2.

https://doi.org/10.1180/mgm.2023.70 Published online by Cambridge University Press

Table 2. Representative trace-element concentrations (LA-ICP-MS, ppm) for narsarsukite from the Papanduva Pluton, Graciosa Province, south-southeastern Brazil.

Sample	MR-02A	MR-06	MR-21	MR-02A(*)
Point_ID	Nar_c1	4_xt3_1c	4_xt2_2c	4_2
Li	n.d.	n.d.	n.d.	37
Be	10	n.d.	19	4
Mg	7	n.d.	n.d.	n.d.
P	n.d.	n.d.	n.d.	n.d.
Ca	n.d.	n.d.	n.d.	n.d.
Sc	13.1	9.3	13.7	9.5
Ti	75,178	75,178	75,178	75,178
V	n.d.	n.d.	n.d.	n.d.
Cr	n.d.	n.d.	n.d.	n.d.
Mn	617	212	826	293
Co	0.02	n.d.	n.d.	n.d.
Cu	1.30	n.d.	n.d.	n.d.
Zn	44	n.a.	n.a.	n.a.
Ga	1.8	2.7	1.3	1.8
Rb	2.8	n.d.	n.d.	0.4
Sr	0.8	n.d.	n.d.	n.d.
Y	2616	859	1776	864
Zr	54,989	3615	5259	4051
Nb	2032	738	1911	1868
Mo	1.30	n.a.	n.a.	n.a.
Sn	374	40	133	111
Cs	1.0	n.d.	n.d.	0.3
Ba	0.6	n.d.	n.d.	5.1
La	0.6	1.3	2.7	24.2
Ce	1.8	6.3	9.4	242.1
Pr	0.6	1.1	1.6	12.8
Nd	6.5	5.5	7.9	59.1
Sm	11	4	4	17
Eu	0.7	0.2	0.2	0.6
Gd	50	17	30	32
Tb	23	5	10	9
Dy	289	84	190	101
Ho	109	32	69	33
Er	493	173	361	140
Tm	111	46	90	25
Yb	1066	473	858	188
Lu	190	91	154	26
Hf	1826	115	205	116
Ta	500	73	241	228
Pb	6	5	5	55
Th	n.d.	n.d.	0.12	0.41
U	0.51	0.46	0.01	2.28

MR-02A, MR-06 and MR-21 = magmatic; MR-2A(*) = post-magmatic, replacing arfvedsonite. n.d. = not detected; n.a. = not analysed. See also Supplementary Table S3.

in all larger and zoned analysed crystals. In the second case, Al increases and Fe^{3+} decreases in a proportion close to 1:1.

In addition to the homovalent substitutions of Ti by Zr and Fe^{3+} by Al, the entry of trivalent cations in the narsarsukite structure is described by the heterovalent substitutions $2R^{4+} = R^{3+} + R^{5+}$ (1) and $R^{4+} + O^{2-} = R^{3+} + F^{1-}$ (2), where R^{3+}, R^{4+} and R^{5+} mainly represent (Al, Fe^{3+}), (Ti, Zr) and Nb, respectively (Wagner *et al.*, 1991; Birkett *et al.*, 1996; Schingaro *et al.*, 2017). These substitutions are plotted in Fig. 6. Wagner *et al.* (1991) also suggested that the substitution $R^{4+} + 2O^{2-} = R^{2+} + 2F^{-1}$ accounts for the entry of divalent cations (Mn, Mg, Ca and Ba), which occur in much lower concentrations in our samples (see Tables 1 and S2). Reaction (1) gives an excellent negative correlation for our dataset, with a determination coefficient $R^2 = 0.93$ (Fig. 6a). However, it plays a minor role in the entry of the R^{3+} cations, as the Nb contents are much lower (≤ 0.036 atoms per formula unit, apfu) than Al and Fe^{3+}, which sum up to 0.456 apfu. Thus, reaction (2), for which we only obtained a moderate negative correlation with a slope of −1.19 and $R^2 = 0.61$ (Fig. 6b), is by far the most important in explaining the observed compositional variations. There are no significant and systematic variations in F or Nb between the magmatic and post-magmatic generations and the higher values of $R^{3+}+F^{1-}$ plotted in Fig. 6b reflect mainly the higher quantities of $Al+Fe^{3+}$ in post-magmatic narsarsukite. The data points have a significant dispersion in this diagram and the slope departs from the ideal value of −1. These features are in part due to the non-consideration of some R^{3+} cations, such as the REE and Y, however it is most probably due to the entry of variable contents of $(OH)^{-1}$ anions in the O site, according to the extended narsarsukite formula suggested by Schingaro *et al.* (2017).

The magmatic and post-magmatic narsarsukite compositions from the Papanduva Pluton are compared in the ternary Fe^{3+}–Al–Zr diagram (Fig. 7) with those of other important worldwide occurrences, which includes peralkaline SiO_2-oversaturated rocks, an alkaline pegmatite from Narsarsuk, the type locality, and hornfels associated with SiO_2-undersaturated rocks (nepheline syenites). They show an extensive variation range that overlaps with most of the available compositions. For example, the magmatic narsarsukite from Papanduva has almost as much Zr as narsarsukite in comendite from the Sirwa Massif, near Ouarzazate (Southern Morrocco), the occurrence with the highest Zr contents reported to date (Wagner *et al.*, 1991). In contrast, the post-magmatic Papanduva narsarsukite can have almost as low Fe^{3+} contents as the specimen in the Illutalik trachyte dyke (Upton *et al.*, 1976), from Illutalik (formerly spelled Igdlutalik) Island, Kujalleq (Greenland). The narsarsukite from lamprophyre dykes of the Murun Massif (Aldan Shield, Russia) has the highest and lowest known Fe^{3+} and Al contents, respectively (Schingaro *et al.*, 2017), whereas the specimen in comendites/pantellerites and related vugs from Mayor Island (New Zealand) present relatively high Zr contents for given Al values (Read, 1991). The Papanduva magmatic narsarsukite has a similar compositional trend to the peralkaline granites from the Strange Lake in northern Québec–Labrador, Canada (Birkett *et al.*, 1996), though with relatively lower Nb and Al and higher Fe^{3+} contents on average. The cores of the largest crystals also have higher Zr contents.

Trace elements

The most abundant trace elements in narsarsukite are the HFSE, Y and the mid to heavy rare earth elements (MREE–HREE), whereas the LILE (large-ion lithophile element) contents are low. In Fig. 8a, we plot selected trace elements normalised to the host rocks for samples MR-2A (magmatic and post-magmatic generations) and MR-21 (magmatic). The post-magmatic narsarsukite from sample MR-2A has higher Ba and light rare earth element (LREE) contents and lower HREE and Hf contents than the magmatic narsarsukite. Tantalum was not plotted in the diagram due to data unavailability for the host rocks, however its abundances range from 38 to 500 ppm and 64 to 268 ppm in magmatic and post-magmatic crystals, and its behaviour closely follows Nb (*cf.* Tables 2 and S3).

The total REE and Y contents of primary narsarsukite range between 505–2353 and 473–2169 ppm, respectively. The post-magmatic crystals have lower contents, ranging from 910–864 ppm (MR-02A) and 602–2165 ppm (MR-06), respectively. The REE patterns of the magmatic generation (Fig. 8b) show high fractionation of the HREE over the LREE and within the HREE and the LREE, with average Ce_N/Yb_N, Ce_N/Sm_N and Gd_N/Yb_N ratios of 0.003, 0.295 and 0.031, respectively, and a strong

https://doi.org/10.1180/mgm.2023.70 Published online by Cambridge University Press

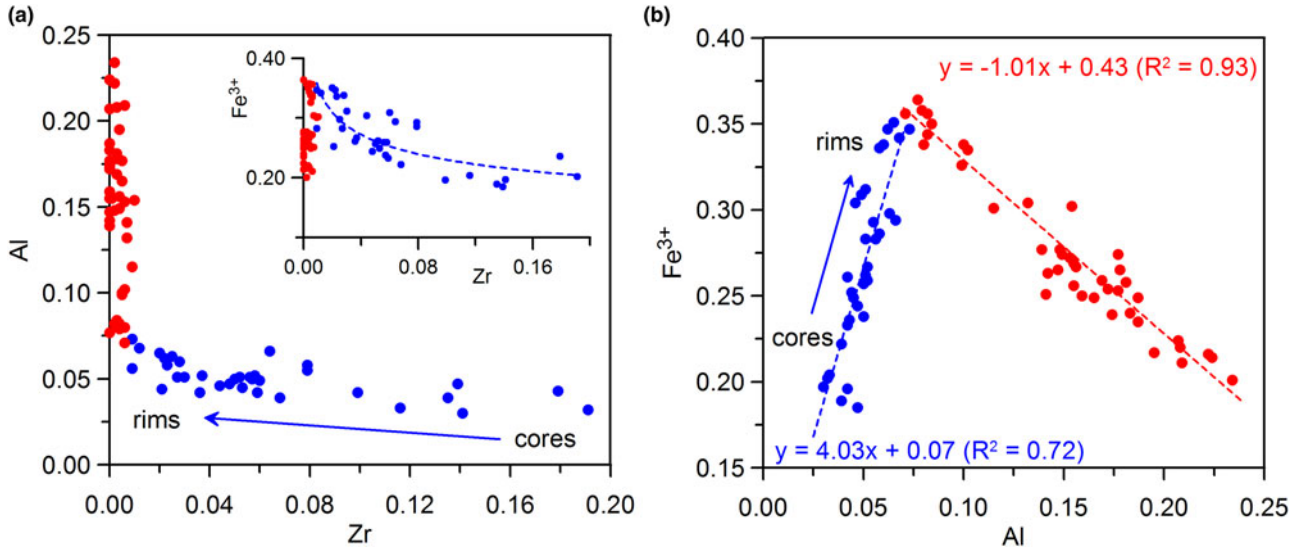

Figure 5. Main compositional variations in narsarsukite from the Papanduva Pluton. (a) Al *vs.* Zr and Fe^{3+} *vs.* Zr (in the inset) and (b) Fe^{3+} *vs.* Al diagram. Note that Fe^{3+} and Al contents show a positive correlation in the magmatic generation, but a negative correlation in the post-magmatic generation. All quantities are expressed in atoms per formula unit (apfu). Colours represent magmatic (blue) and post-magmatic (red) generations.

negative Eu anomaly, with an average Eu* [$=Eu_N/(Sm_N*Gd_N))^{0.5}$] = 0.09. The post-magmatic crystals have a relatively flat distribution pattern, with a similar Eu anomaly. The average data for the Strange Lake narsarsukite (Vasyukova and Williams-Jones, 2019) is also plotted in Fig. 8b for comparison. This shows considerably higher total REEs and Y (averaging 14,453 and 4872 ppm, respectively), with a significant high-fractionated average pattern and a less pronounced negative Eu anomaly.

Discussion and final remarks

Textures and compositions of narsarsukite

Narsarsukite is a common accessory in strongly peralkaline granites from the Papanduva Pluton. It formed both in the magmatic and the post-magmatic crystallisation environments. Late-magmatic, relatively larger and compositionally zoned crystals were followed by poikilitic intergrowths between narsarsukite and albite formed in the latest melt pockets. Similar aegirine + albite, arfvedsonite + albite, and aenigmatite + albite intergrowths occur in the Papanduva Pluton. The albite laths within these intergrowths are almost pure (Ab ≥ 98% molar) and have significantly high Fe_2O_3 contents (Vilalva, 2007). These intergrowths suggest co-precipitation of these phases and closely resemble the so-called khibinitic texture typical of the SiO_2-undersaturated eudialyte-bearing, agpaitic, nepheline syenites (khibinites, e.g. Gerasimovsky *et al.*, 1974; Ulbrich and Ulbrich, 2000). Therefore, albite (as an Al_2O_3-saturated phase) stabilised at the end of the magmatic crystallisation. Conversely, the fibrous narsarsukite crystals or crystals aggregates that appear

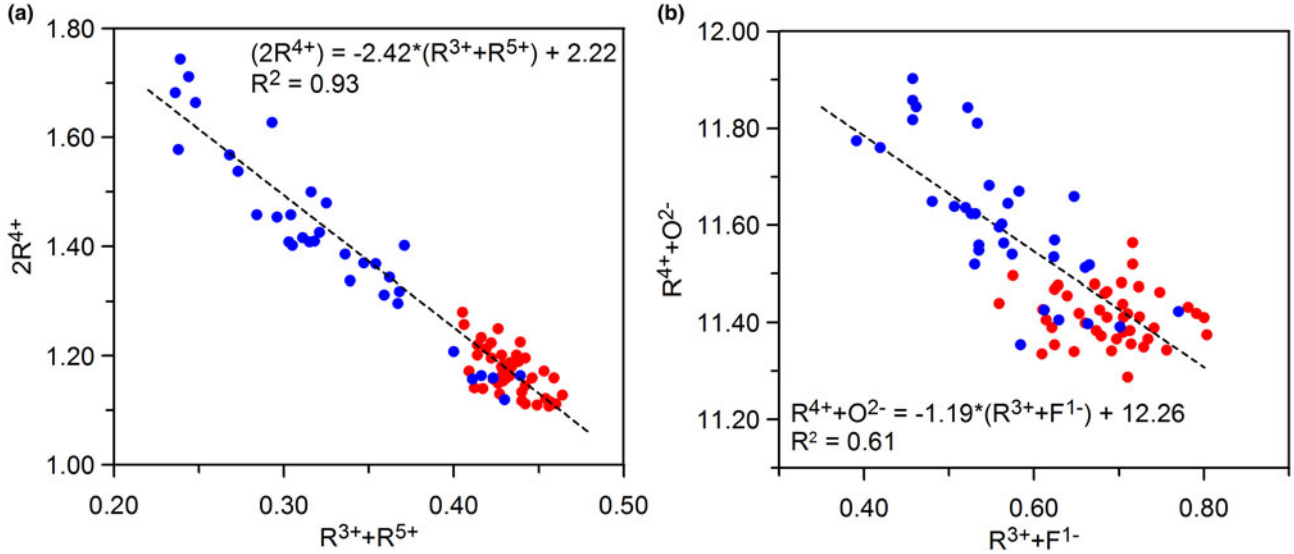

Figure 6. Heterovalent substitution mechanisms accounting for the main compositional variations for Papanduva narsarsukite. (a) $2R^{4+}$ *vs.* $R^{3+}+R^{5+}$. (b) $R^{4+}+O^{2-}$ *vs.* $R^{3+}+F^{1-}$ plot. R^{3+}, R^{4+} and R^{5+} are (Al, Fe^{3+}), (Ti, Zr) and Nb, respectively. Symbols as in Fig. 5. See text.

https://doi.org/10.1180/mgm.2023.70 Published online by Cambridge University Press

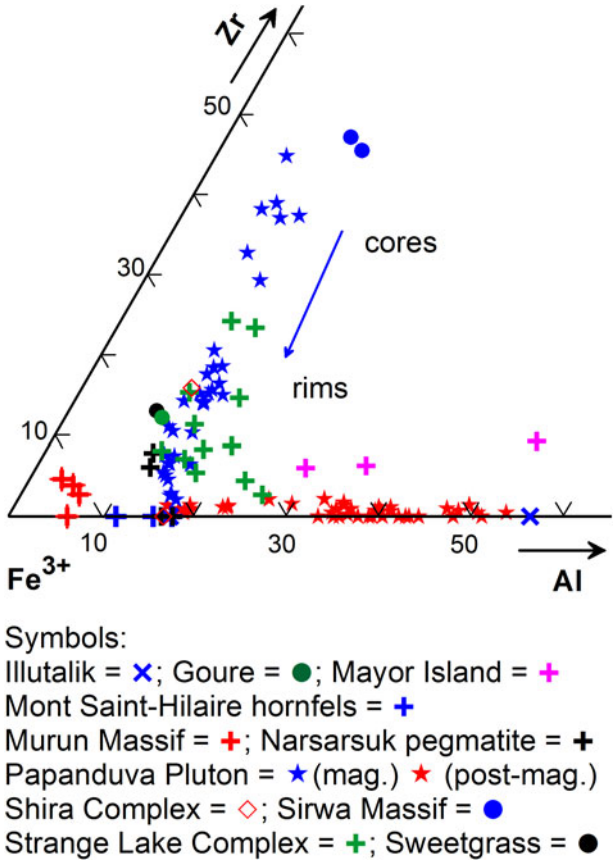

Figure 7. Fe^{3+}–Al–Zr ternary diagram showing the compositional trends for the magmatic and post-magmatic narsarsukite from the Papanduva Pluton, compared with worldwide available compositions in peralkaline SiO_2-oversaturated rocks, pegmatites and hornfels associated with nepheline syenites. Data sources: Illutalik dyke (Kujalleq, Greenland): Upton *et al.* (1976); Gouré region (Niger): Jérémine and Christophe-Michel-Lévy (1961); Mayor Island (Bay of Plenty region, New Zealand) and Mont Saint-Hilaire hornfels (southern Quebec, Canada): Read (1991); Murun Massif (Aldan Shield, Russia): Schingaro *et al.* (2017); Narsarsuk pegmatite (type area, Narsarsuk, Kujalleq, Greenland) and Sirwa Massif (north of Ouarzazate, Southern Morrocco): Wagner *et al.* (1991); Shira Complex (northern Nigeria): Bennet *et al.* (1984); Papanduva Pluton: this work; Strange Lake granites (northern Québec-Labrador, Canada): Birkett *et al.* (1996); Sweetgrass Hills (north-central Montana, USA): Graham (1935, *in* Wagner *et al.*, 1991). See text.

interstitially or replace arfvedsonite and aegirine are typically post-magmatic (hydrothermal).

The Papanduva narsarsukite covers the compositional range for Fe^{3+}, Al and Zr described in the literature. A well-defined Fe^{3+} inflection marks the compositional limit between the magmatic and the post-magmatic generations, with the latter being Zr-poor and Al-rich. This inflection reflects that Fe^{3+} was less available in the fluids and preferentially partitioned into other Fe^{3+}-bearing phases, such as aegirine (*cf.* below). The increasing contribution of Al-bearing late fluids also contributed to this inflection. The relative proportions for the main R^{4+}, R^{3+} and R^{5+} cations and O^{2-} and F^{1-} suggest the presence of some $(OH)^{1-}$ anions in the O site, in agreement with the findings of Schingaro *et al.* (2017).

The narsarsukite investigated has significant total REE and Y (up to 2350 and 2170 ppm) contents. However, these contents are considerably lower than those reported for the narsarsukite in the Strange Lake Complex (Vasyukova and Williams-Jones, 2019), which also has highly fractionated REE patterns and smaller negative Eu anomalies. This difference could be due to the higher contents of HFSE and REE in the granites from Strange Lake, or to the occurrence of a different set of accessories competing for the REE and Y. The REE and other R^{3+} cations enter the six-fold coordinated [Ti]-site, which is significantly distorted in narsarsukite (Schingaro *et al.*, 2017). The effective ionic radii (Shannon, 1976) of $^{VI}Ti^{4+}$ is 61 pm, and this explains the increasing preference for the smaller HREE in this site. However, even $^{VI}Lu^{3+}$, the smallest REE, has an effective radius (~86 pm), significantly higher than $^{VI}Ti^{4+}$, and this limits the maximum REE and Y contents in narsarsukite. The REE patterns obtained for the hydrothermal crystals replacing amphibole are characterised by relatively flat distribution patterns with higher LREE abundances, characteristics that are similar to those observed in hydrothermal zircon (e.g. Hoskin, 2005; Vlach, 2022).

The replacement of arfvedsonite and aegirine by narsarsukite

The replacement of arfvedsonite and possibly aegirine by narsarsukite during the post-magmatic crystallisation stage suggests the involvement of relatively Ti-rich late fluids in the mineralogical evolution of the host granites. This is supported by the occurrence of hydrothermal Ti-minerals such as neptunite, titanite and anatase in miarolitic cavities and vugs within the granites (Vilalva, 2007).

In this sense and considering idealised end-members, narsarsukite might be formed through the following replacement reactions:

$$2[Na_3Fe_4^{2+}Fe^{3+}Si_8O_{22}(OH,F)_2]_{Arf} + 3[TiO_2]_{Fluid} + 3O_2 = 3[Na_2TiSi_4O_{11}(OH,F)]_{Nar} + 5[Fe_2O_3]_{Hem} + 4[SiO_2]_{Qz} + [(OH,F)]_{Fluid} \quad (1)$$

and

$$2[NaFeSi_2O_6]_{Aeg} + [TiO_2]_{Fluid} + [(OH,F)]_{Fluid} = [Na_2TiSi_4O_{11}(OH,F)]_{Nar} + [Fe_2O_3]_{Hem} \quad (2)$$

The hydrothermal replacement of arfvedsonite by narsarsukite is probably favoured in relatively oxidising conditions. If Na metasilicate ($Na_2Si_2O_5$) or a similar compound and SiO_2 species are available in the fluid, aegirine will be formed preferentially instead of hematite, according to the reaction:

$$[Fe_2O_3]_{Hem} + [Na_2Si_2O_5]_{Fluid} + 2[SiO_2]_{Fluid} = 2[NaFeSi_2O_6]_{Aeg} \quad (3)$$

Importantly, the occurrence of contrasted magmatic and hydrothermal aegirine generations and hydrothermal aegirine replacing arfvedsonite are standard features in these rocks (e.g. Vilalva *et al.*, 2016; Vasyukova and Williams-Jones, 2019).

The compositions of the involved primary and post-magmatic crystallising phases can be used to infer the compositional characteristics of the post-magmatic fluid. The average compositions of arfvedsonite and primary aegirine in the narsarsukite-bearing granites are given in Supplementary Table S4 (see complete data set in Vilalva *et al.*, 2016). In a gain–loss diagram (Fig. 9), the replacing narsarsukite has higher contents of Be, Al, Sc, Ba, HFSE, Y, REE, Th, U and Pb, in addition to Ti, Na, Al and Si, than arfvedsonite. This suggests that the fluid phase was relatively

https://doi.org/10.1180/mgm.2023.70 Published online by Cambridge University Press

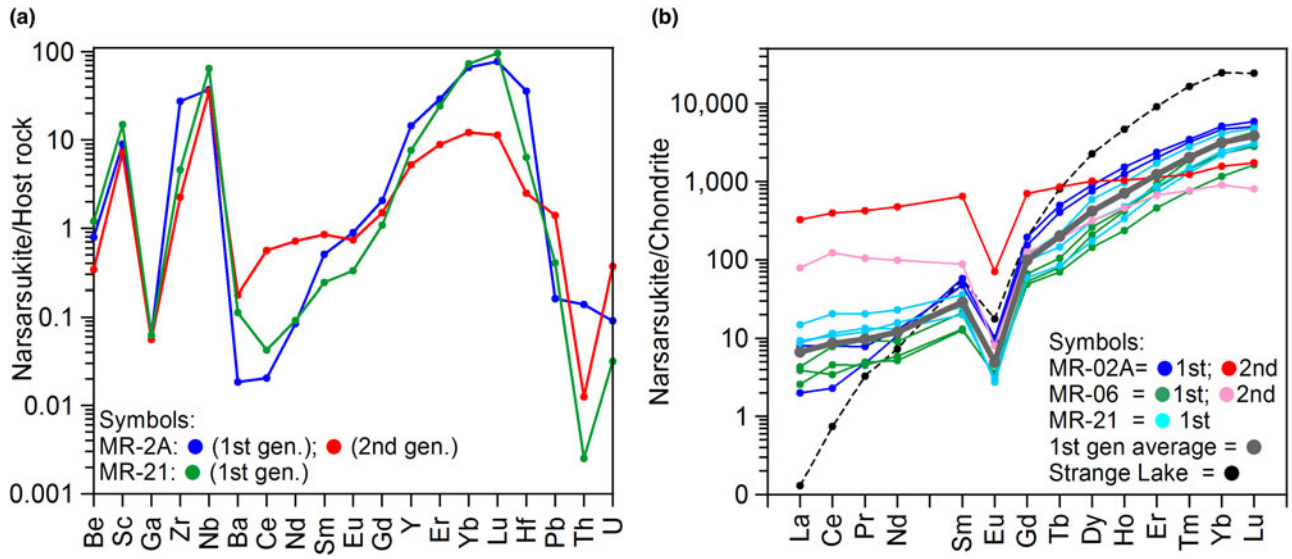

Figure 8. (a) Multi-element diagram showing the behaviour of selected trace elements in magmatic (1st gen.) and post-magmatic (2nd gen.) narsarsukite, normalised to the respective host rocks. Average data are presented for the magmatic generation; for the post-magmatic case, this is the only reliable result for this sample. Host-rock data from Vilalva and Vlach (2014). (b) REE patterns for magmatic (1st) and post-magmatic (2nd) narsarsukite from the Papanduva Pluton. Strange Lake data from Vasyukova and Williams-Jones (2019). Normalisation factors from Boynton (1984). See text.

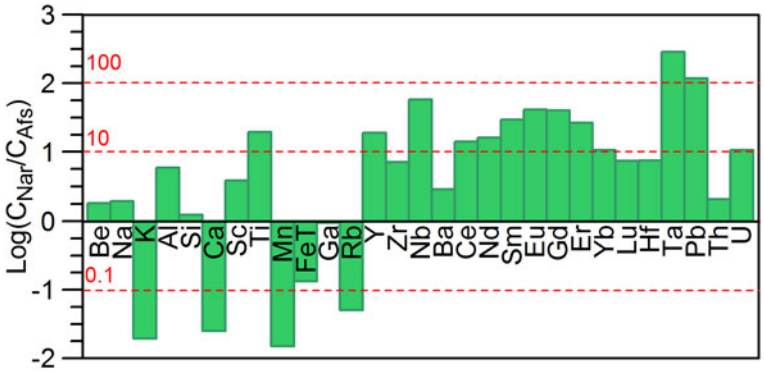

Figure 9. Gain-loss diagram illustrating the ratios between major, minor and trace element concentrations, expressed as $\log(C_{Nar}/C_{Afs})$, for the post-magmatic narsarsukite and the replaced arfvedsonite shown in Fig. 3i. The red lines correspond to the indicated actual concentration ratios (C_{Nar}/C_{Afs}).

enriched in these elements. Conversely, K, Ca, Mn, Fe and Rb were released preferentially from the amphibole to the fluid phase.

Narsarsukite in peralkaline granites and a comment on the use of the term agpaitic

Narsarsukite is a significant and widely distributed primary accessory phase in some highly peralkaline granites such as those from the Papanduva Pluton and the Strange Lake Complex. It should be included as a characteristic and diagnostic Na–Ti-bearing mineral in the assemblages of these rocks, together with other rare Ti- and Zr-minerals, such as aenigmatite, astrophyllite and elpidite.

Given the inherent difficulties and compositional complexities, experimental constraints on the crystallisation of narsarsukite and other rare Na–K–Ti–Zr-bearing phases starting from peralkaline SiO_2-oversaturated compositions are rare or absent. Upton *et al.* (1976) simulated the crystallisation of a narsarsukite-bearing peralkaline trachyte under 100 MPa and saturated H_2O conditions at the magnetite–hematite buffer, however narsarsukite was not observed among the products. A qualitative analysis on the relative stability of narsarsukite and other Ti-minerals for the Strange Lake case was presented by Birkett *et al.* (1996), based on chemographic relations in the Na–Fe^{2+}–Fe^{3+}–Ti space.

The term 'agpaitic' was introduced by Ussing (1912) for some nepheline syenites from the Ilímaussaq Complex (south Greenland). It is specifically recommended for peralkaline nepheline syenites containing complex Zr- and Ti-silicate minerals, with corresponding particular geochemical signatures (see also Sørensen, 1960; Le Maitre, 1989). However, Vlach and Gualda (2007) used the this term to describe the mineralogy of the most evolved peralkaline granites in the Papanduva Pluton considering the widespread occurrence of titano- and zirconosilicate among the rare accessory phases. Later, Marks *et al.* (2011) proposed to extend the term 'agpaitic' to include peralkaline granitic rocks with (K, Ti)-, (K, Zr)-, (Na, Ti)- and (Na, Zr)-bearing rare mineral assemblages such as eudialyte + aenigmatite, astrophyllite + dalyite, aenigmatite + dalyite and astrophyllite + dalyite. We agree with Marks *et al.* (2011) and believe that these highly peralkaline granites, together with rhyolites, containing rare Zr- and Ti-silicate minerals might also be characterised as agpaitic to distinguish them from more common peralkaline SiO_2-oversaturated rocks. However this proposal needs to be

https://doi.org/10.1180/mgm.2023.70 Published online by Cambridge University Press

discussed further by the petrological community and is beyond the scope of this work.

Acknowledgements. The authors are grateful to staff of the GeoAnalitica facility for analytical support during laboratory work and to Fundação de Amparo à Pesquisa do Estado de São Paulo, FAPESP (Grant 2019/17343-4) for funding this research. The comments and suggestions of two anonymous referees and the Associate Editor helped to improve the manuscript and are greatly appreciated.

Supplementary material. The supplementary material for this article can be found at https://doi.org/10.1180/mgm.2023.70.

Competing interests. The authors declare none.

References

Andersen T., Erambert M., Larsen A.O. and Selbekk R.S. (2010) Petrology of nepheline syenite pegmatites in the Oslo Rift, Norway: Zirconium silicate mineral assemblages as indicators of alkalinity and volatile fugacity in mildly agpaitic magma. *Journal of Petrology*, **51**, 2303–2325.

Andrade S. (2016) *Análises por LA-ICPMS em zircões de rochas graníticas da Faixa Ribeira no Estado de São Paulo—SE Brasil: Implicações genéticas e geocronológicas*. Doctoral Thesis, University of São Paulo, São Paulo, Brazil, 361 pp. [in Portuguese].

Anthony J.W., Bideaux R.A., Bladh K.W. and Nicchols M.C. (editors) (2003) *Handbook of Mineralogy*. Mineralogical Society of America, Chantilly, Virginia, USA.

Balmer M.L., Bunker B.C., Wang L.Q., Peden C.H.F. and Su Y. (1997) Solid-state ^{29}Si MAS NMR study of titanosilicates. *The Journal of Physical Chemistry B*, **101**, 9170–9179.

Bastin G.F. and Heijligers H.J.M. (1990) Progress in electron-probe microanalysis. *Materialwissenschaft und Werkstofftechnik*, **21**, 90–92.

Bennet J.N., Turner E.C., Ike C. and Bowden P. (1984) The geology of some northern Nigerian anorogenic ring complexes. *Overseas Geology and Mineral Resources*, **61**, 1–65.

Birkett T., Trzcienski Jr. W.E. and Stirling J.A.R. (1996) Occurrence and composition of some Ti-bearing minerals in the Strange Lake Intrusive Complex, Quebec-Labrador Boundary. *The Canadian Mineralogist*, **34**, 779–801.

Boynton W.V. (1984) Cosmochemistry of the rare earth elements: meteorite studies. Pp. 63–114 in *Rare Earth Element Geochemistry* (P. Henderson, editor). Elsevier, Amsterdam.

Day M. and Hawthorne F. (2020) A structure hierarchy for silicate minerals: Chain, ribbon, and tube silicates. *Mineralogical Magazine*, **84**, 165–244.

Flink G. (1901) Undersögelser af minerallen fra Julianehaab, Pt. 1, On the minerals from Narsarsuk on the Firth of Tunugdlliarfik in Southern Greenland. *Meddeleser om Grönland*, **24**, 9–180.

Gerasimovsky V.I., Volkov V.P, Kogarko L.N. and Polyakov A.l. (1974) Kola Peninsula. Pp. 206–220 in *The Alkaline Rocks* (H. Sørensen, editor). Wiley, New York.

Graham W.A.P. (1935) An occurrence of narsarsukite in Montana. *American Mineralogist*, **20**, 598–601.

Griffin W.L., Powell W.J., Pearson N.J. and O'Reilly S.Y. (2008) GLITTER: data reduction software for laser ablation ICP–MS. Pp. 204–207 in: *Laser Ablation ICP–MS in the Earth Sciences* (P. Sylvester, editor). Mineralogical Association of Canada Short Course Series Volume 40.

Gualda G.A.R. and Vlach S.R.F. (2007) The Serra da Graciosa A-type granites and syenites, southern Brazil. Part 1: Regional setting and geological characterization. *Anais da Academia Brasileira de Ciências*, **79**, 405–430.

Hoskin P.W.O. (2005) Trace-element composition of hydrothermal zircon and the alteration of Hadean zircon from the Jack Hills, Australia. *Geochimica et Cosmochimica Acta*, **69**, 637–648.

Jérémine E. and Christophe Michel-Lévy M. (1961) Un noveau gisement de narsarsukite. *Bulletin de la Société Française de Minéralogie et Christallographie*, **84**, 191–194.

Le Maitre R.W. (ed) (1989) *A Classification of Igneous Rocks and Glossary of Terms*. Blackwell Scientific Publications, Oxford, 193 pp.

Marks M.A.W., Hettmann K., Schilling J., Frost B.R. and Markl G. (2011) The mineralogical diversity of alkaline igneous rocks: Critical factors for the transition from miaskitic to agpaitic phase assemblages. *Journal of Petrology*, **52**, 439–455.

Nicholls J. and Carmichael I.S.E. (1969) Peralkaline acid liquids: a petrological study. *Contributions to Mineralogy and Petrology*, **20**, 268–294.

Peacor D.R. and Buerger M.J. (1962) The determination and refinement of the structure of narsarsukite, $Na_2TiOSi_4O_{10}$. *American Mineralogist*, **47**, 539–556.

Pyatenko Y.A. and Pudovkina Z.V. (1960) Crystal structure of narsarsukite. *Soviet Physics Crystallography*, **5**, 540–548.

Rainho J.P., Lin Z., Rocha J. and Carlos L.D. (2003) Synthesis and luminescence of Eu^{3+}-doped narsarsukite prepared by the sol-gel process. *Journal of Sol-Gel Science and Technology*, **36**, 1005–1009.

Read A.J. (1991) Narsarsukite from Mayor Island, New Zealand. *Journal of Geology and Geophysics*, **34**, 337–340.

Schingaro E., Mesto E., Lacalamita M., Scordari F., Kaneva E. and Vladykin F.N. (2017) Single-crystal X-ray diffraction, EMPA, FTIR and X-ray photoelectron spectroscopy study of narsarsukite from Murun Massif, Russia. *Mineralogical Magazine*, **81**, 339–354.

Shannon R.D. (1976) Revised effective ionic radii and systematic studies of interatomic distances in halides and chalcogenides. *Acta Crystallographica*, **A32**, 751–767.

Siachoque A., Vilalva F.C.J. and Vlach S.R.F. (2022) Astrophyllite in peralkaline granites from the Graciosa Province (S-SE Brazil): Insights from magmatic vs post magmatic crystallization environments. *Lithos*, 432–433, 106892. https://doi.org/10.1016/j.lithos.2022.106892.

Sørensen H. (1960) On the agpaitic rocks. Pp. 319–327 in *Report of the International Geological Congress Twenty First Session, Norden, Copenhagen, Denmark, Volume 13: Petrographic Provinces, Igneous and Metamorphic Rocks*.

Ulbrich H.H. and Ulbrich M.N.C. (2000) The lujavrite and khibinite bodies in the Poços de Caldas Alkaline Massif, Southeastern Brazil: a structural and petrographic study. *Revista Brasileira de Geociências*, **30**, 615–622.

Upton B.G.J., Macdonald R., Hill P.G., Jefferies B. and Ford S.E. (1976) Narsarsukite: a new occurrence in peralkaline trachyte, South Greenland. *Mineralogical Magazine*, **40**, 737–746.

Ussing N.V. (1912) Geology of the country around Julianehaab, Greenland. *Meddelelser om Grønland*, **38**, 1–376.

Vasyukova O.V. and Williams-Jones A.E. (2019) Closed system fluid-mineral-mediated trace element behaviour in peralkaline rare metal pegmatites: evidence from Strange Lake. *Chemical Geology*, **505**, 86–99.

Vilalva F.C.J. (2007) *Petrografia e mineralogia de granitos peralkalinos: O Pluton Papanduva, Complexo Morro Redondo (PR/SC)*. Master's Dissertation, University of São Paulo, São Paulo, Brazil [in Portuguese].

Vilalva F.C.J. and Vlach S.R.F. (2010) Major- and trace-element composition of REE-rich turkestanite from peralkaline granites of the Morro Redondo Complex, Graciosa Province, south Brazil. *Mineralogical Magazine*, **74**, 645–658.

Vilalva F.C.J. and Vlach S.R.F. (2014) Geology, petrography and geochemistry of the A-type granites from the Morro Redondo Complex (PR–SC), southern Brazil, Graciosa Province. *Anais da Academia Brasileira de Ciências*, **86**, 85–116.

Vilalva F.C.J., Vlach S.R.F. and Simonetti A. (2013) Nacareniobsite-(Ce) and britholite-(Ce) in peralkaline granites from the Morro Redondo Complex, Graciosa Province, southern Brazil: occurrence and compositional data. *The Canadian Mineralogist*, **51**, 313–332.

Vilalva F.C.J., Vlach S.R.F. and Simonetti A. (2016) Chemical and O-isotope compositions of amphiboles and clinopyroxenes from A-type granites of the Papanduva Pluton, South Brazil: Insights into late- to post-magmatic evolution of peralkaline systems. *Chemical Geology*, **420**, 186–199.

Vilalva F.C.J., Simonetti A. and Vlach S.R.F. (2019) Insights on the origin of the Graciosa A-type granites and syenites (Southern Brazil) from zircon U–Pb geochronology, chemistry, and Hf and O isotope compositions. *Lithos*, **340–341**, 20–33.

Vlach S.R.F. (2022) On the morphology and geochemistry of hydrothermal crypto- and microcrystalline zircon aggregates in a peralkaline granite. *Minerals*, **12**, 628. https://doi.org/10.3390/min12050628.

Vlach S.R. and Gualda G.A. (2007) Allanite and chevkinite in A-type granites and syenites of the Graciosa Province, southern Brazil. *Lithos*, **97**, 98–121.

Vlach S.R.F., Siga O., Harara O.M.M., Gualda G. A.R., Basei M.A.S and Vilalva F.C.J. (2011) Crystallization ages of the A-type magmatism of the Graciosa Province (Southern Brazil): Constraints from zircon U–Pb (ID–TIMS) dating of coeval K-rich gabbro–dioritic rocks. *Journal of South American Earth Sciences*, **32**, 407–415.

Wagner C., Parodi G.C., Semet M., Robert J.L. Berrahma M. and Velde D. (1991) Crystal chemistry of narsarsukite. *European Journal of Mineralogy*, **3**, 575–585.

Warr L.N. (2021) IMA-CNMNC approved mineral symbols. *Mineralogical Magazine*, **85**, 291–320.

https://doi.org/10.1180/mgm.2023.70 Published online by Cambridge University Press